

Simultaneous blockade of a photon phonon, and magnon induced by a two-level atom

Chengsong Zhao,¹ Xun Li,^{1,2} Shilei Chao,¹ Rui Peng,¹ Chong Li,¹ and Ling Zhou^{1,*}

¹*School of Physics, Dalian University of Technology, Dalian 116024, China*

²*National Key Laboratory of Shock Wave and Detonation Physics, Institute of Fluid Physics, China Academy of Engineering Physics, Mianyang 621900, China*

The hybrid microwave optomechanical-magnetic system has recently emerged as a promising candidate for coherent information processing because of the ultrastrong microwave photon-magnon coupling and the longlife of the magnon and phonon. As a quantum information processing device, the realization of single excitation holds special meaning for the hybrid system. In this paper, we introduce a single two-level atom into the optomechanical-magnetic system and show that an unconventional blockade due to destructive interference cannot offer a blockade of both the photon and magnon. Meanwhile under the condition of single excitation resonance, the blockade of photon, phonon, and magnon can be achieved simultaneously even in a weak optomechanical region, but the phonon blockade still requires the cryogenic temperature condition.

I. INTRODUCTION

The effect of one photon preventing the second photon entrance is called a photon blockade [1, 2], which is the pivotal effect to achieve photons at the quantum level. It is believed that photon blockade can be used as a single photon source and to process quantum information [3]. The photon blockade in the cavity-QED systems [4–6] were thoroughly investigated and have been achieved in experiments [7, 8]. Recently, the optomechanical system has attracted significant attention, such as working as a sensor to detect tiny mass and force [9–12], a platform to investigate the fundamental physics [13] and a device to processing quantum information [14–20]. The most attractive characteristic of an optomechanical system is the nonlinearity resulting from the radiation pressure, which can induce Kerr nonlinearity [21] and produce the photon blockade [22]. However, currently, the single-photon optomechanical coupling is still within a weak coupling region, which only induces only fainter Kerr nonlinearity. Therefore, some strategies were put forward to enhance the nonlinearity [23, 24]. To avoid the weakness of the delicate single-photon nonlinear coupling, the photon blockade resulting from destructive interference called unconventional blockade (UB) was proposed and thoroughly investigated [25, 26].

Most recently, the photon-magnon coupling system in the microwave [27–29] and optical frequency [30–32] regime has aroused attention. Different from the weak optomechanical coupling, the ultrastrong coupling between microwave photons and magnons [the collective spin excitation in yttrium iron garnet (YIG)] was realized [28, 33], and the magnons possess a very low damping rate. Meanwhile, the magnon excitation interacting with phonons (vibrational modes of the YIG sphere) is similar to the optomechanical interaction, [34], so, both kinds of interactions magnetic-mechanical [35] and optical-mechanical are nonlinear. The phonons and

magnons posse coupling mediated by cavity fields [36], and the entanglement of a magnon, photon, and phonon in cavity magnomechanics has been investigated where photon-magnon and magnomechanical interactions were considered [34]. In Ref. [37], the supermode of a photon exhibits blockade under the Kerr effect in optomagnonic microcavities system.

The photon blockade can be generated from the destructive interference [25, 38] as well as the single excitation resonance [6, 21, 39–41]. Usually, the destructive interference and the single excitation resonance resulting from dressed states can supply a better blockade than the Kerr effect because of the weak coupling strength of the Kerr interaction. The photon blockade in an optomechanical system [25] as well as in an optomagnonic system [37] were separately thoroughly investigated. A magnon blockade via qubit-magnon coupling has been studied in Ref. [42]. However, in the hybrid optomechanical-magnetic system, the simultaneous blockade of the photon, phonon, and magnon has not been studied. Meanwhile, the hybrid system has special significance for the realization of quantum information processing, like the quantum internet [43]. If the hybrid optomechanical-magnetic system was used as a quantum device, the single excitation level is important, and the simultaneous blockade of photon, phonon, and magnon should be pivotal and deserves further investigation.

In this paper, we consider a hybrid microwave optomechanical-magnetic system aiming to generate the simultaneous photon-phonon-magnon blockade. Considering the achievement of ultrastrong microwave optical-magnetic coupling in experiments [27, 44], we derive three-partite interaction among photon, phonon, and magnon. By introducing a single two-level atom, under the condition of single excitation resonance, we show that the simultaneous blockade of photon, phonon, and magnon can be achieved with the assistance of the three-partite interaction on the condition of cryogenic temperature of the mechanical mode, while the unconventional destructive interference can not offer the simultaneously multi-modes antibunching. In our scheme the single-photon strong optomechanical coupling is not required,

* zhlhxn@dlut.edu.cn

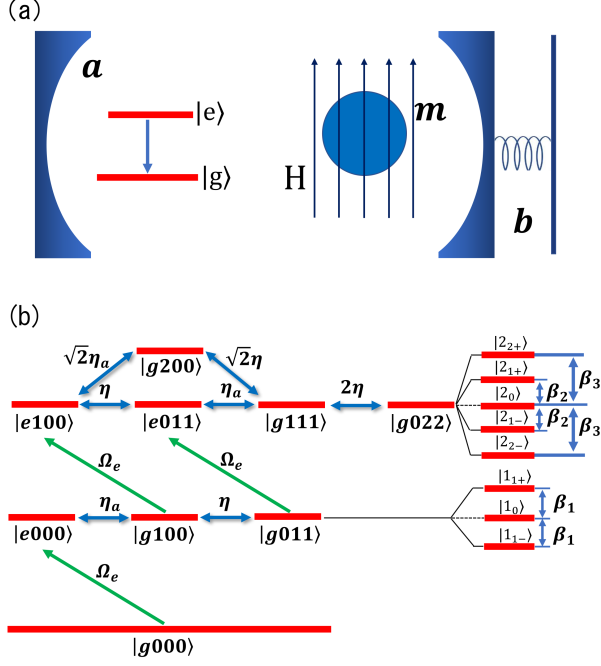


FIG. 1. (a) Sketch of the system. A two-level atom is placed inside a microwave cavity with a movable mirror. A YIG sphere is placed near the maximum magnetic field of the cavity mode, and in a uniform bias magnetic field, which establishes the magnon-photon coupling. (b) Energy-level diagram under the Hamiltonian Eq. (3), where $|g(e), n_+, n_-, n_b\rangle$ denotes lower-level g (upper level e), and $n_j (j = +, -, b)$ is the number of the mode (a_+, a_-, b) . The eigenstates are drawn on the right-hand side.

therefore, it can be feasible in experiment. Our scheme is a guideline for hybrid optomechanical-magnetic experiments nearing the regime of single-photon nonlinearity, and for potential quantum information processing applications with photons, magnons, and phonons.

II. THE MODEL AND THE ANALYTICAL ANALYSIS

We consider a hybrid optomechanical-magnetic system, where a two-level atom and a YIG microsphere are contained in the microwave cavity, and one of the mirrors is movable, shown in Fig. 1(a). The magnons are sourced from a collective spins in a ferrimagnet. Here, we ignore the interaction between magnons and phonons due to deformation of the YIG sphere, because the single-magnon magnomechanical coupling rate is typically small [34, 36]. The magnetic dipole mediates the coupling between magnons and cavity photons. The Hamiltonian of the system reads

$$H = H_{om} + H_{op} + H_{ao} + H_d, \quad (1)$$

where

$$\begin{aligned} H_{om} &= \omega_c a^\dagger a + \omega_m m^\dagger m + G_m (a^\dagger m + a m^\dagger), \\ H_{op} &= \omega_b b^\dagger b + g a^\dagger a (b^\dagger + b), \\ H_{ao} &= \omega_a \sigma^\dagger \sigma + g_a (\sigma a^\dagger + \sigma^\dagger a), \\ H_d &= \Omega_e (\sigma e^{i\omega_L t} + \sigma^\dagger e^{-i\omega_L t}), \end{aligned} \quad (2)$$

$j^\dagger (j, j = a, m, b)$ is the creation (annihilation) operator of the related mode (photon, magnon, and phonon) with frequency ω_c , ω_m and ω_b , respectively. σ stands for the pseudo-spin of the two-level atom. H_{om} consists of the energy of the photon and magnon, as well as the photon-magnon interaction with the effective strength G_m , which is called the cavity magnon polaritons [45]. H_{op} is composed of the energy of the phonon and the optomechanical interaction with coupling strength g . The first term in H_{ao} is the energy of the atom, and the second term describes the atom interacting with the cavity field. H_d denotes an atom pumped with a classical field with frequency ω_L .

In the frame rotating with $H_0 = \omega_L (a^\dagger a + \sigma^\dagger \sigma + m^\dagger m)$, the Hamiltonian can be changed into time-independent. For simplicity, we assume $\omega_m = \omega_c$, then $\delta = \omega_{c(m)} - \omega_L$. We diagonalize the Hamiltonian $H'_0 = \delta (a^\dagger a + m^\dagger m) + G_m (a^\dagger m + a m^\dagger)$ by introducing supermodes $a_\pm = \frac{1}{\sqrt{2}} (a \pm m)$. Considering photon-magnon interaction larger than the optomechanical and atom-photon interaction, i.e., $G_m \gg \{g, g_a\}$ and choosing $\omega_b = 2G_m$, we rewrite the Hamiltonian as

$$\begin{aligned} H_{eff} &= \Delta a_+^\dagger a_+ + (\Delta - 2G_m) a_-^\dagger a_- + \omega_b b^\dagger b + \Delta_a \sigma^\dagger \sigma \\ &\quad - \eta (a_+^\dagger a_- b + a_+ a_-^\dagger b^\dagger) + \eta_a (a_+^\dagger \sigma + a_+ \sigma^\dagger) \\ &\quad + \Omega_e (\sigma + \sigma^\dagger), \end{aligned} \quad (3)$$

where $\Delta = \delta + G_m$, $\eta = g/2$, $\eta_a = g_a/\sqrt{2}$, $\Delta_a = \omega_a - \omega_L$. The detailed deduction of Hamiltonian (3) is given in Appendix A. For simplicity, hereafter we will assume $\Delta = \Delta_a$. We see that the effective Hamiltonian contains three-partite interaction, which is similar to in Ref. [25]. Differently from their scheme, we introduce a pumped two-level atom aiming to achieve a blockade of the photon, magnon, and phonon. We also would like to compare the different effect of a blockade between the destructive interference mechanism and the single excitation resonance mechanism. Observe the last two brackets in Eq. (3); the pumped two-level atom interacts with mode a_+ , which results in the blockade of mode a_+ . Although the three-partite nonlinear interaction means the parametric-down conversion form between a_- and b mediated by absorption or emission of mode a_+ , the blockade of the mode a_+ can not result in the amplification in mode a_- and b . Instead, if there is only one excitation in the mode a_+ , the transfer of the single excitation creates only one excitation in every mode of a_- and b , that is to say, the blockade in mode a_+ will lead to the blockade in mode a_- and mode b ; therefore it is possible to generate a blockade in supermodes a_+ , a_- and mode b . We will

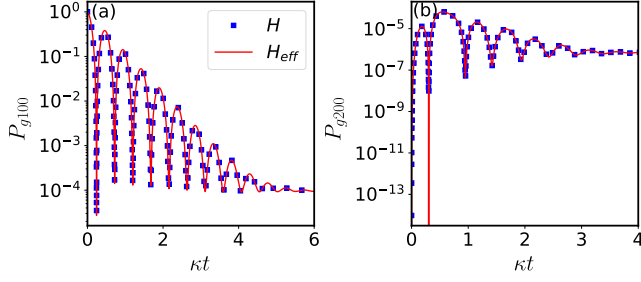


FIG. 2. The evolution of probabilities P_{g100} (a) and P_{g200} (b) with original Hamiltonian H (red line) and effective Hamiltonian H_{eff} (blue squares), respectively, where $P_{g100} = |C_{g100}|^2$, $P_{g200} = |C_{g200}|^2$. The parameters are $\eta = 5\kappa$, $\eta_a = 6/\sqrt{2}\kappa$, $G_m = 200\kappa$, and $\Omega_e = 0.1\kappa$.

show that the bare modes a , b , and m can also be blockaded simultaneously.

To check the validity of the approximation from Hamiltonian (1) to Hamiltonian (3), we choose $|g100\rangle$ as the initial state and plot the evolution of the probabilities of states $|g200\rangle$ and $|g100\rangle$ governed by the Hamiltonians H and H_{eff} respectively, shown in Fig. 2, where $|e(g), n_+, n_-, n_b\rangle$ represents a state with atom in $|e\rangle$ ($|g\rangle$), and $|n_+\rangle$, $|n_-\rangle$, and $|n_b\rangle$ are the number state for the a_+ , a_- , and b modes, respectively. From Fig. 2, we see clearly that the results of original Hamiltonian agree very well with that of effective Hamiltonian H_{eff} , which means that the effective Hamiltonian H_{eff} is reliable.

Due to the limit of the weak driving field, for understanding the blockade mechanism of the photon (phonon, magnon), we temporarily ignore the pumping of the atom and derive the eigenstates and eigenvalues of H_{eff} (3) in the few-photon subspace, yielding

$$\begin{aligned}
 |0\rangle : \lambda_0 &= 0, \\
 |1_0\rangle : \lambda_{10} &= \Delta, \\
 |1_{\pm}\rangle : \lambda_{1\pm} &= \Delta \pm \beta_1, \\
 |2_0\rangle : \lambda_{20} &= 2\Delta, \\
 |2_{1\pm}\rangle : \lambda_{21\pm} &= 2\Delta \pm \beta_2, \\
 |2_{2\pm}\rangle : \lambda_{22\pm} &= 2\Delta \pm \beta_3,
 \end{aligned} \tag{4}$$

where $\beta_1 = \sqrt{\eta_a^2 + \eta^2}$, $\beta_2 = \sqrt{\frac{3\eta_a^2 + 7\eta^2 - D}{2}}$, $\beta_3 = \sqrt{\frac{3\eta_a^2 + 7\eta^2 + D}{2}}$, $D = \sqrt{\eta_a^4 + 26\eta_a^2\eta^2 + 25\eta^4}$. The expression of the dressed states $|s_c\rangle$ ($s = 0, 1, 2$; $c = 0, \pm, 1\pm, 2\pm$) is given in Appendix A, and the energy-levels are shown on the right side of Fig. 1(b).

In the weak driving limit, to analytically derive the equal-time second-order correction function, the state of the system can be truncated in few excitation subspace and approximately expressed as

$$\begin{aligned}
 |\psi\rangle &= C_{g000}|g000\rangle + C_{g100}|g100\rangle + C_{g011}|g011\rangle \\
 &+ C_{e000}|e000\rangle + C_{g200}|g200\rangle + C_{g111}|g111\rangle \\
 &+ C_{e100}|e100\rangle + C_{g022}|g022\rangle + C_{e011}|e011\rangle.
 \end{aligned} \tag{5}$$

Under the action of the non-Hermitian Hamiltonian $\tilde{H} = H_{eff} - i(\kappa_+ a_+^\dagger a_+ + \kappa_- a_-^\dagger a_- + \kappa_a \sigma^\dagger \sigma)$ with the decay rate κ_j ($j = +, -, a$), the probability amplitude in $|\psi\rangle$ can be obtained by solving the Schrödinger equation $i\partial|\psi\rangle/\partial t = \tilde{H}|\psi\rangle$. The detail of the deduction and the steady-state solution can be found in Appendix B.

To characterize nonclassical photon (magnon, phonon) statistics, we employ an equal-time second-order correlation function defined by

$$g_i^2(0) = \frac{\text{Tr}(c_i^\dagger c_i^\dagger c_i c_i \rho)}{[\text{Tr}(c_i^\dagger c_i \rho)]^2}, \tag{6}$$

where $i = a, m, b, a_+, a_-$. The steady-state correlation functions of our system can be analytically obtained via the steady-state wave function (5) as

$$\begin{aligned}
 g_{a_+}^2(0) &= \frac{2|C_{g200}|^2}{(|C_{g100}|^2 + u_1)^2} \approx \frac{2|C_{g200}|^2}{|C_{g100}|^4}, \\
 g_{a_-}^2(0) &= \frac{2|C_{g022}|^2}{(|C_{g011}|^2 + u_2)^2} \approx \frac{2|C_{g022}|^2}{|C_{g011}|^4},
 \end{aligned} \tag{7}$$

with $u_1 = 2|C_{g200}|^2 + |C_{g111}|^2 + |C_{e100}|^2$, and $u_2 = 2|C_{g022}|^2 + |C_{g111}|^2 + |C_{e011}|^2$ where the second approximate equals in Eq. (7) are obtained under the conditions $|C_{g000}| \gg \{|C_{g100}|, |C_{g011}|, |C_{e000}|\} \gg \{|C_{g200}|, |C_{g111}|, |C_{g022}|, |C_{e100}|, |C_{e011}|\}$. For mode b , it is not reasonable to obtain $g_b^2(0)$ with the analytical solution (5) because its decay has been ignored. We will directly calculate it from the master equation. The correlation function $g_i^2(0) \geq 1$ is referred to as Poissonian and super-Poissonian. The correlation function $g_i^2(0) < 1$ indicates sub-Poissonian, and the limit $g_i^2(0) \rightarrow 0$ corresponds to the complete blockade. Remarkably, the single-photon regime is usually characterized by $g_i^2(0) < 0.5$ [38]. From the expression Eq. (7) and Eq. (B2), one can see that the blockade in mode a_+ (a_-) is possible only if the population C_{g200} (C_{g022}) ≈ 0 . We will plot second-order correlation function and discuss it further in the next section.

Although the polariton modes [45–47] consisting of optical mode and magnetic mode can be indirectly derived by directly detecting the output spectrum of photons, the blockade of the photon, phonon, and magnon still deserve our investigation. Due to the combination of the optical mode and magnetic mode, the statistical properties of supermodes a_{\pm} and bare modes a and m are different. In order to see clearly the difference, we derive

the relations between the two bases

$$\begin{aligned}
|00\rangle_d &= |00\rangle, \\
|10\rangle_d &= \frac{1}{\sqrt{2}}(|10\rangle + |01\rangle), \\
|01\rangle_d &= \frac{1}{\sqrt{2}}(|10\rangle - |01\rangle), \\
|02\rangle_d &= \frac{1}{2}(|20\rangle - \sqrt{2}|11\rangle + |02\rangle), \\
|20\rangle_d &= \frac{1}{2}(|20\rangle + \sqrt{2}|11\rangle + |02\rangle), \\
|11\rangle_d &= \frac{1}{\sqrt{2}}(|20\rangle - |02\rangle),
\end{aligned} \tag{8}$$

where the left side states are labeled by $|n_+, n_-\rangle_d$ (n_+ and n_- correspond to the Fock state of mode a_+ and a_-) while right-side state are labeled with $|n_m, n_a\rangle$ (n_m and n_a denote the Fock state of mode m and a). The derivation of Eq. (8) is given in Appendix C. See the last line in Eq. (8), where the state $|11\rangle_d$ means only one excitation in mode a_+ and a_- , however for the modes m and a , they might be populated in two excitations. That is to say, the blockade of supermodes a_+ and a_- does not mean the blockade of bare modes a and m . Therefore, we need to calculate the second-order correlation of the mode m and a :

$$\begin{aligned}
g_a^2(0) &\approx \frac{2(|C_{g200}|^2 + |C_{g022}|^2 + 2|C_{g111}|^2)}{(|C_{g100}|^2 + |C_{g011}|^2)^2}, \\
g_m^2(0) &= g_a^2(0).
\end{aligned} \tag{9}$$

We can see that the correlation functions for the optical and magnetic mode are the same. The blockades in the modes m and a require that C_{g200} , C_{g022} and C_{g111} reach zero simultaneously. Fortunately, as one can observe from Eq. (B2), when C_{g022} equals zero, C_{g111} is equal to zero too. That is to say, when both a_+ and a_- modes are a blockade, the photon and magnon modes a and m are both a blockade too.

III. THE STATISTICAL PROPERTIES OF THE MULTIMODE FIELD

In the above analytical calculation of $g_i^2(0)$ ($i = a_{\pm}, b, a, m$), we have made some approximations. We now show the correction of the approximations and investigate the statistical properties of the multimode field. For simplicity, we assume that the decay rates of the optical mode, magnetic mode, and atom are equal, and then we can derive the master equation as

$$\begin{aligned}
\dot{\rho} &= -i[H_{eff}, \rho] + \kappa(\mathcal{D}[a_+] + \mathcal{D}[a_-] + \mathcal{D}[\sigma])\rho \\
&\quad + (n_{th} + 1)\kappa_b\mathcal{D}[b]\rho + n_{th}\kappa_b\mathcal{D}[b^\dagger]\rho,
\end{aligned} \tag{10}$$

where ρ is the density matrix of the hybrid system, $\mathcal{D}[o]\rho = 2o\rho o^\dagger - o^\dagger o\rho - \rho o^\dagger o$, and n_{th} is the thermal phonon population. We assume that the average particle

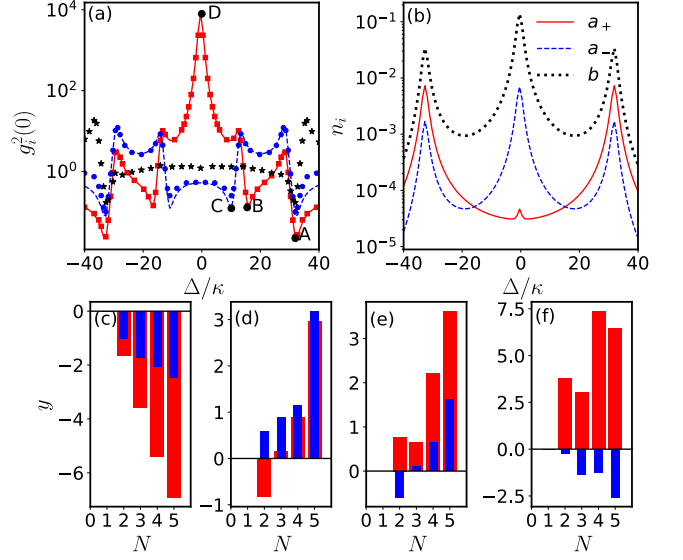


FIG. 3. (a) Equal-time second-order correlation function for modes a_+ (red solid, red square), a_- (blue dashed, blue dot), and b (black asterisk) versus detuning Δ , where lines and marks represent analytical and numerical solutions respectively. (b) The average particle number. The relative probability population function y (c)-(f) corresponding to the mark point A-D in (a), where red (light gray) and blue (dark gray) bars represent supermode a_+ and a_- , respectively. The parameters are $\eta_a = 40/\sqrt{2}\kappa$, $\eta = 15\kappa$, $\kappa_b = 0.05\kappa$, $\Omega = 0.1\kappa$, $G_m = 800\kappa$, and $n_{th} = 0$.

numbers of photons (magnons) in thermal equilibrium are zero because of their high frequencies.

We truncate the Fock space up to $|5\rangle$ for modes a_{\pm} and b . Based on the subspace consisting of the two-level atom and the modes a_{\pm} and b , we numerically solve Eq. (10) and calculate the second-order correlation function of mode a_{\pm} and b . In Fig. 3(a), we plot $g_{a_{\pm}}^2(0)$ with an analytical solution of Eqs. (7) and numerical results of Eq. (10), respectively. We see that they agree well, which means that we can understand the second order correlation with the analytic analysis. In order to make clear the relation between the mechanism of blockade and the probability distribution, we define the function $y(N) = \log_{10} \frac{P(N)}{P_p(N)}$ where $P(N)$ is the probability in $|N\rangle$, and $P_p(N)$ is Poissonian distribution; thus the value of y reveals the relative difference between the population and Poissonian distribution. In Fig. 3(c) to 3(f), we plot $y(N)$ corresponding to point A to D respectively. If y is positive, population at N excitation is higher than Poissonian distribution, or otherwise it is lower than the Poissonian distribution.

For the mark point A in Fig. 3(a), $\Delta = \beta_1$, $\lambda_{1-} = 0$, which means the single excitation resonance. Then $|1_-\rangle$ can be easily populated (for the symmetry point of A, $\Delta = -\beta_1$, $\lambda_{1+} = 0$, then $|1_+\rangle$ is easy to be populated). Notice the expression $|1_-\rangle$ in Eq. (A6), where there

is only one excitation in modes a_{\pm} and b , so we can see strong blockade in a_+ , a_- , and b modes under the same condition. Meanwhile the average numbers n_{a_+} , n_{a_-} , and n_b reach their local maximum of $n_{a_{\pm}(b)}$ [see Fig. 3(b)]. All of the probability at $N > 1$ is less than Poissonian distribution due to the resonance mechanism, shown in Fig. 3(c).

For the mark point B in Fig. 3(a), $g_{a_{\pm}}^2(0)$ achieves a local minimum value where the real part of numerator of C_{g200} is zero. By observing Fig. 1(b), the two jumps $|e100\rangle \rightarrow |g200\rangle$ and $|g111\rangle \rightarrow |g200\rangle$ destructively interfere each other, such that the population in $|g200\rangle$ is low, so the mode a_+ is blockade. That is the so-called UB. However, under this condition, the a_- mode is super-Poissonian because there is a population in $|g111\rangle$, resulting in population $|g022\rangle$. By observing Fig. 3(d), the destructive interference only decreases the probability in $N = 2$ for the mode a_+ , while for the mode a_- the probability for $N > 1$ is higher than Poissonian distribution. This result indicates that the destructive interference can not offer blockade for both supermodes a_+ and a_- .

For the point C in Fig. 3(a), $g_{a_{\pm}}^2(0)$ achieves a local minimum value. As one can observe from Eq. (B2), the requirement for $C_{g022} \approx 0$ is the same as that for $C_{g111} \approx 0$, if $\{\eta, \eta_a\} \neq 0$. As seen in Fig. 1(b), there are two jumps $|g200\rangle \rightarrow |g111\rangle$ and $|e011\rangle \rightarrow |g111\rangle$. Their destructive interference results in blockade in mode a_- . Meanwhile, there is a population in the state $|g200\rangle$, which means the super-Poissonian in mode a_+ . Correspondingly, in Fig. 3(e), the population of mode a_+ is still higher than the Poissonian distribution, while for the mode a_- , the destructive interference only decrease the probability in only $N = 2$. This result is similar to what we have pointed in the analysis of point B, i.e., the destructive interference can not offer us a simultaneous blockade in supermode a_+ and a_- .

For the point D, in Fig. 3(a), $\Delta = 0$, $\lambda_{10} = \lambda_{20} = 0$, which means that the single excitation resonance $|1_0\rangle$ and double resonant excitation $|2_0\rangle$ are both satisfied. Observing Eq. (A6), the resonance between state $|1_0\rangle$ and state $|0\rangle$ can lead to the populations in the states $|g011\rangle$ and $|e000\rangle$. Likewise, the population in $|2_0\rangle$ means that the states $|g200\rangle$, and $|e011\rangle$ are easily populated too, while the state $|g022\rangle$ is not so easily populated because of the mutual cancellation between η and η_a [the factor $\frac{\eta_a^2 - \eta^2}{\sqrt{2}\eta^2 A_1}$ is smaller than $\frac{\eta_a}{\beta_1}$, see Eq. (A6)]. Therefore, the mode a_+ will be strong super-Poissonian, and the mode a_- is sub-Poissonian. The results are corresponding to Fig. 3(f), where the population for mode a_+ is higher than the Poissonian distribution, and the probabilities distribution for mode a_- are less than Poissonian.

As we have mentioned before, for mode b , $g_b^2(0)$ should not be calculated from an analytical solution Eq. (5). We directly calculate $g_b^2(0)$ with the master equation (10), shown in Fig. 3(a). We see that around point A, we can also achieve blockade in mode b . Therefore, under single excitation resonance, all of the modes a_+ , a_- , and b exhibit the blockade phenomenon. In addition, the param-

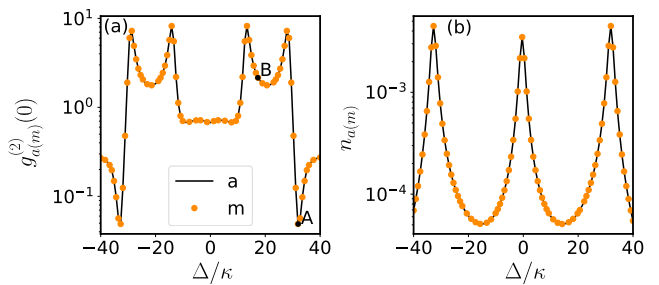


FIG. 4. (a): Equal time second correlation function for modes a (solid line), m (dots). (b): average number for optical mode a (solid line) and magnetic mode m (dots) as functions of detuning Δ . The other parameters are the same as in Fig. 3.

eters, in Fig. 3, $\frac{g^2}{\omega_b \kappa} = 9/16 < 1$ means that weak photon nonlinearity from radiation pressure in an optomechanical system could generate a photon, magnon, and phonon blockade, in our system. But the single-photon optomechanical coupling g is still larger than the damping rate κ . We will show that the single excitation resonant does not require $g > \kappa$; that is to say, even under the condition $g < \kappa$, we still can obtain the simultaneous blockade for the three modes.

In Fig. 4, we plot $g_a^2(0)$ (solid) and $g_m^2(0)$ (dots), where, obviously, they are the same and agree well with Eq. (9). As we have analyzed before, the blockade of a_+ mode means $|C_{g200}|^2 \approx 0$, and the a_- mode blockade corresponds to $|C_{g022}|^2 \approx 0$ (also $|C_{g111}|^2 \approx 0$). When both a_+ and a_- modes are a blockade, from the expression Eq (9), the photon a and the magnon m are both blockade; therefore at point A [see Fig. 4(a)], the optical mode and magnetic mode are both a blockade. However, around $\Delta = 0$ (point D), the statistical property of $g_{a_{\pm}}^2(0)$ is different from that of $g_{a_{\pm}}^2(0)$, $g_{a(m)}^2(0)$ still showing sub-Poissonian. From Eqs. (8), (9), and (B2), we obtain

$$g_a^2(0) \approx \frac{1}{F_2^2} g_{a_+}^2(0) + \left(\frac{2}{F_1} - \frac{1}{F_1^2}\right) g_{a_-}^2(0), \quad (11)$$

where $F_1 = |\frac{\tilde{\Delta}}{\eta}|^2 + 1$, $F_2 = |\frac{\eta}{\tilde{\Delta}}|^2 + 1$, and $\tilde{\Delta} = \Delta - i\kappa$. So, when Δ is extremely small, $F_1 \rightarrow 1$ and $F_2 \rightarrow \infty$, then, $g_a^2(0)$ is dominated by $g_{a_-}^2(0)$. Therefore, we can observe a sub-Poissonian around $\Delta = 0$ regime. Comparing the value of $g_{a(m)}^2(0)$ around point B with that around point A, we see that the sub-Poissonian resulting from destructive interference (point B) does not exist, but the blockade resulting from single excitation resonance (point A) still exists.

To further characterize the blockade of modes a_{\pm} , b , a , and m , choosing a single excitation resonance condition $\Delta = \beta_1$, we plot a second-order delay correlation function defined by $g_i^{(2)}(\tau) = \frac{\langle c_i^\dagger(0)c_i^\dagger(\tau)c_i(\tau)c_i(0) \rangle}{\langle c_i^\dagger(0)c_i(0) \rangle^2}$ in Fig. 5. $g_i^{(2)}(\tau) \leq g_i^2(0)$ is called bunching, and $g_i^{(2)}(\tau) > g_i^2(0)$ is called antibunching which is also the quantum signature [48]. Meanwhile, $g^2(\tau)$ is proportional

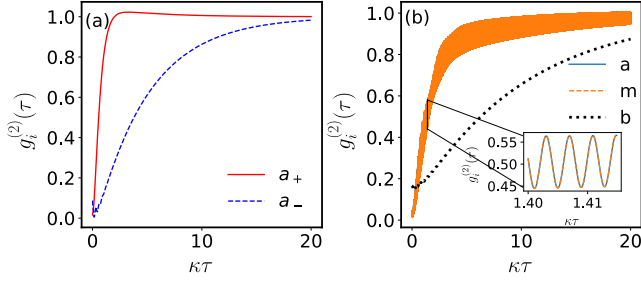


FIG. 5. Time-delay second-order correlation function for supermode a_+ (red solid line) and a_- (blue dashed line) in (a), and for optical mode (blue solid line), magnetic mode (orange dashed line), and mechanical mode (black dotted line) in (b). We set $\Delta = \beta_1$, and other parameters are the same as in Fig. 3. The panel in (b) shows the partial enlarged detail.

to the condition probability for detecting a second photon (magnon, phonon) at $t = \tau$, given that a photon (magnon, phonon) has been detected earlier at $t = 0$ [49]. Observing Figs. 5(a) and (b), because of the single excitation resonance, the time-delay correction functions for supermodes a_{\pm} and optical, magnetic, or mechanical mode are all antibunching even in the weak photon nonlinear region. $g_m^{(2)}(\tau)$ agrees well with $g_a^{(2)}(\tau)$ which is just like the equal-time second-order correlation function. Comparing Figs. 5(a) and (b), the time-delay correction function of supermodes a_{\pm} has no quick oscillations, but that of the optical and magnetic mode exhibits quick oscillations. The quick local oscillations in the time-delay second-order function for optical and magnetic mode results from the interference between supermodes a_+ and a_- and the frequency of mechanical mode b [39].

We now investigate the second-order correlation function $g_{a(m)}^{(2)}$ affected by the coupling strength η_a shown in Fig. 6. From Figs. 6(a) and (b), we observe that with the increasing of η_a , the low value $\log_{10}g_a^{(2)}(0)$ points (single excitation resonance) in terms of Δ are increased, which is because the resonant condition $\Delta = \beta_1$ is increased with η_a . In Fig. 6(b), interestingly, the minimum value of $g_{a(m)}^{(2)}$ is not monotonous decreasing with increasing η_a . When $\eta_a \approx 17.7\kappa$, $g_{a(m)}^{(2)}$ is abnormal where the effect of the single excitation resonance does not result in a blockade as in the other case. See the mark point P in Fig. 6(a), where there is a cross where the $\Delta = \beta_1$ (the single excitation resonance) and $\Delta = \beta_2/2$ (two excitation resonance) are both satisfied, so, $g_{a(m)}^{(2)}$ can not show a blockade. Except for the cross point, the larger value of η_a , the better the blockade.

We now show that it is possible to generate a photon, magnon, and phonon blockade without a strong optomechanical coupling coefficient. In Fig. 7, both $\frac{g^2}{\omega_b\kappa} \ll 1$ and $g < \kappa$ are satisfied, and we plot the equal-time second-order correlation function for modes b , a , and m . In Fig. 7(a), due to single excitation resonance, the strong sub-Poissonian for modes a , m , and b can be observed,

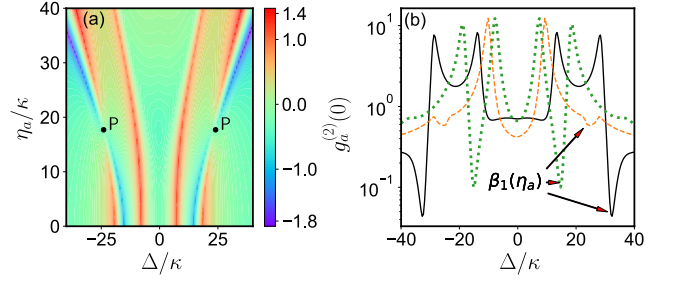


FIG. 6. (a): Contour plot $\log_{10}g_a^{(2)}(0)$ as function of η_a and Δ . (b): $g_a^{(2)}(0)$ change with Δ for several values of $\eta_a = 40/\sqrt{2}\kappa$ (black solid line), 17.7κ (orange dashed line), 0.5κ (green dotted line). The other parameters are the same as in Fig. 3

while the destructive interference resulting in a blockade is not observed in the weak coupling regime. Here, although the single-photon optomechanical coupling is small, the large atom-photon interaction g_a makes β_1 larger than κ , which ensures the blockade of the photon, magnon, and phonon. We can understand it from Eq.(B2). In order to keep single excitation, the denominator of C_{g100} (C_{g011}, C_{e000}) should be as low as possible, i.e., $\min|\Delta^2 - \eta^2 - \eta_a^2|$, then we deduce the condition $\Delta = \sqrt{\eta^2 + \eta_a^2 - \kappa^2}$. Therefore, even $\eta < \kappa$, the relative large value of η_a still can make $\eta^2 + \eta_a^2 > \kappa^2$, and then the single excitation will dominate the wave function, and the blockade can be obtained. We can conclude that the single excitation resonance can result in a multimode blockade even in a weak optomechanical coupling region while the destructive interference can not offer us multimode antibunching.

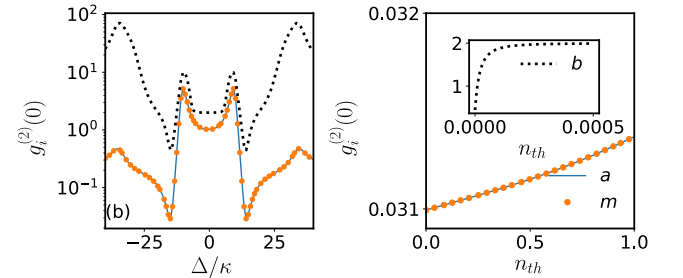


FIG. 7. (a) Equal-time second-order correlation function for mode a (blue solid line), m (orange dots), and b (black dotted line). We set $\eta = 0.2\kappa$, $\Omega_e = 0.8\kappa$, $\eta_a = 20/\sqrt{2}\kappa$, and $\kappa_b = \kappa$ in (a). The other parameters are same as in Fig. 3. (b) Equal-time second-order correlation function versus thermal phonon population. We set $\Delta = \beta_1$, and other parameters are the same as in panel (a).

In Fig. 7(b), we plot the equal-time second-order correlation functions of a photon, magnon, and phonon affected by thermal phonon number. As we can observe the blockade of a photon and magnon under a weak coupling regime still exists after considering the thermal environment of a phonon, but the phonon blockade disappears

and the correlation function approaches 2 with increasing n_{th} . When the thermal phonon population is taken into account, the state of the system truncated in the few excitation subspace can be expressed as mixed state of $|\psi_n\rangle$ [25] where

$$\begin{aligned} |\psi_n\rangle = & C_{g00n}|g00n\rangle + C_{g10n}|g10n\rangle + C_{g0n+1}|g01n+1\rangle \\ & + C_{e00n}|e00n\rangle + C_{g20n}|g20n\rangle + C_{g11n+1}|g11n+1\rangle \\ & + C_{e10n}|e10n\rangle + C_{g02n+2}|g02n+2\rangle \\ & + C_{e01n+1}|e01n+1\rangle. \end{aligned} \quad (12)$$

Because of the three-partite interaction $a_+a_-^\dagger b^\dagger + h.c.$, the thermal phonon cannot be converted into a photon and magnon. From Eq. (12), although the thermal phonon can be in the state $|n\rangle$, the states of photon and magnon still can be in $|0\rangle$ or $|1\rangle$, which means the blockade of modes a and m still exists, but phonon blockade will be destroyed ($n > 1$) [42, 50–52], and the correlation function of the phonon will close to the that of thermal field. But, the blockade of the photon and magnon is affected slightly by the thermal environment because of the change in the single excitation resonance for $|\psi_n\rangle$ [25]. Therefore, to generate simultaneous blockade of a photon, phonon, and magnon, the small thermal phonon population is necessary.

IV. DISCUSSION AND CONCLUSION

When the single excitation resonance condition is satisfied, The simultaneous blockade of a photon, phonon and magnon can offer us some potential applications. The usual hybrid system mainly contains two different physical systems, but the quantum internet may require more complex quantum information processing, like the processing and storing of information while simultaneously updating the information in a quantum information circuit and network [43]. The simultaneous blockade of a multimode field could be used in this process and be more powerful than the usual single mode blockade. If we realize the single excitation, from Eq. (8), the photon and magnon will be a in Bell state $1/\sqrt{2}(|10\rangle \pm |01\rangle)$, which is useful in quantum information processing.

From Fig. 3 to Fig. 7, the parameter G_m is seemingly not important in numerical simulation, but we do need strong magnon-photon coupling, because we require the condition $G_m \gg \{\eta, \eta_a\}$ to achieve the effective Hamiltonian, and the three-partite interaction is true only under this condition. Recently, strong and even ultrastrong coupling between photons and magnons at microwave frequencies, using of a YIG sphere, has been reported [27, 28]. For instance, in Ref. [27], the magnon-photon coupling strength was achieved as high as $g = 2\pi \times 2.5\text{GHz}$, and dissipation rates of the microwave photon and the magnon resonance are $\kappa_a = 2\pi \times 33\text{MHz}$ and $\kappa_m = 2\pi \times 15\text{MHz}$, respectively. Currently, the optomechanical single-photon

strong-coupling condition $g > \kappa$ is still a challenge. Most of the experiments of the optomechanical system are still within the single-photon weak coupling regime [17, 53, 54]. In our scheme, the three-partite interaction is results from the optomechanical interaction, but the single-photon strong coupling is not necessary.

In this paper, we put forward a scheme to generate a photon, phonon and magnon blockade in a hybrid microwave optomechanical-magnetic system. By introducing a two-level atom interacting with the cavity field, we carefully compare the blockade resulting from destructive interference and that resulting from single excitation resonance. We find that the blockade resulting from single excitation resonance is much better than that resulting from destructive interference. Most importantly, under the same detuning condition, the photon, phonon and magnon can be blockade simultaneously. Furthermore, we find that the phonon blockade is easy to be destroyed by thermal excitation, while the blockade of the photon and magnon are affected slightly by the thermal environment. To generate simultaneous blockade of the photon, phonon and magnon, the small thermal phonon population is necessary.

In our system, the multipartite interaction results from optomechanical coupling, which is the key factor to obtain the simultaneous blockade of the photon, phonon, magnon. However, the single excitation is the condition of the simultaneous blockade, and the single-photon strong optomechanical coupling condition is not required. Therefore, the present scheme is feasible in experiment, which is a guideline for hybrid optomechanical-magnetic experiments nearing the regime of single-photon nonlinearity, and for potential quantum information processing applications with photons, magnons and phonons.

ACKNOWLEDGEMENTS

We are grateful to J.Q. You and Guo-Qiang Zhang for enlightening discussions. This work was supported by NSFC under Grant No. 11874099.

Appendix A: The derivation of an effective Hamiltonian and its eigenstates

In this appendix, we give the detailed derivation for Hamiltonian (3). In the frame rotating with $H_0 = \omega_L(a^\dagger a + \sigma^\dagger \sigma + m^\dagger m)$, the Hamiltonian (1) can be written as

$$\begin{aligned} H = & \delta_c a^\dagger a + \delta_m m^\dagger m + G_m(a^\dagger m + am^\dagger) \\ & + \omega_b b^\dagger b + g a^\dagger a (b^\dagger + b) \\ & + \Delta_a \sigma^\dagger \sigma + g_a (\sigma a^\dagger + \sigma^\dagger a) \\ & + \Omega_e (\sigma + \sigma^\dagger), \end{aligned} \quad (A1)$$

with $\delta_{c(m)} = \omega_{c(m)} - \omega_L$. For simplicity, we assume $\omega_m = \omega_c$, then $\delta_c = \delta_m = \delta$. We diagonalize the Hamil-

tonian $H'_0 = \delta(a^\dagger a + m^\dagger m) + G_m(a^\dagger m + am^\dagger)$ by introducing $a_\pm = \frac{1}{\sqrt{2}}(a \pm m)$, then $H'_0 = (\delta + G_m)a^\dagger_+ a_+ + (\delta - G_m)a^\dagger_- a_-$. Choosing $H_{f0} = \Delta a^\dagger_+ a_+ + (\Delta - 2G_m)a^\dagger_- a_- + \omega_b b^\dagger b + \Delta_a \sigma^\dagger \sigma$ and assuming $\omega_b = 2G_m$, $\Delta = \Delta_a$, we switch into the interaction picture and obtain

$$H_I = \eta(a^\dagger_+ a_+ + a^\dagger_- a_- - a^\dagger_+ a_- e^{i2G_m t} - a^\dagger_- a_+ e^{-i2G_m t}) \\ \times (be^{-i\omega_b t} + b^\dagger e^{i\omega_b t}) + \Omega_e(\sigma e^{-i\Delta t} + \sigma^\dagger e^{i\Delta t}) \\ + \eta_a(a^\dagger_+ \sigma + a_+ \sigma^\dagger - a^\dagger_- \sigma e^{-i2G_m t} - a_- \sigma^\dagger e^{i2G_m t}), \quad (\text{A2})$$

where $\eta_a = \frac{g_a}{\sqrt{2}}$, $\eta = \frac{g}{2}$. The detuning Δ can be arbitrary value. Considering $G_m \gg \{\eta, \eta_a\}$, we take rotating wave approximation and ignore high frequency terms, then the Hamiltonian could be written as

$$H_I = -\eta(a^\dagger_+ a_- b + a^\dagger_- a_+ b^\dagger) + \eta_a(a^\dagger_+ \sigma + a_+ \sigma^\dagger) \\ + \Omega_e(\sigma e^{i\Delta t} + \sigma^\dagger e^{-i\Delta t}). \quad (\text{A3})$$

We would like to rewrite the Hamiltonian into time-independent form by switching back into original picture, then we have

$$H_{eff} = \Delta a^\dagger_+ a_+ + (\Delta - 2G_m)a^\dagger_- a_- + \omega_b b^\dagger b + \Delta_a \sigma^\dagger \sigma \\ - g_a/2(a^\dagger_+ a_- b + a^\dagger_- a_+ b^\dagger) \\ + g/\sqrt{2}(a^\dagger_+ \sigma + a_+ \sigma^\dagger) + \Omega_e(\sigma + \sigma^\dagger). \quad (\text{A4})$$

It is exactly the effective Hamiltonian (3).

In the limit of a weak driving field, we temporary forget the pumping of the atom and derive the eigenstates and eigenvalues of H_{eff} in the few-photon subspace, yielding

$$\begin{aligned} |0\rangle : \lambda_0 &= 0, \\ |1_0\rangle : \lambda_{10} &= \Delta, \\ |1_\pm\rangle : \lambda_{1\pm} &= \Delta \pm \beta_1, \\ |2_0\rangle : \lambda_{20} &= 2\Delta, \\ |2_{1\pm}\rangle : \lambda_{21\pm} &= 2\Delta \pm \beta_2, \\ |2_{2\pm}\rangle : \lambda_{22\pm} &= 2\Delta \pm \beta_3, \end{aligned} \quad (\text{A5})$$

where $\beta_1 = \sqrt{\eta_a^2 + \eta^2}$, $\beta_2 = \sqrt{\frac{3\eta_a^2 + 7\eta^2 - D}{2}}$, $\beta_3 = \sqrt{\frac{3\eta_a^2 + 7\eta^2 + D}{2}}$, $D = \sqrt{\eta_a^4 + 26\eta_a^2\eta^2 + 25\eta^4}$. The corre-

sponding eigenstates are

$$\begin{aligned} |0\rangle &= |g000\rangle, \\ |1_0\rangle &= \frac{1}{\beta_1}(\eta_a |g011\rangle + \eta |e000\rangle), \\ |1_- \rangle &= \frac{1}{\sqrt{2}}(|g100\rangle + \frac{\eta}{\beta_1} |g011\rangle - \frac{\eta_a}{\beta_1} |e000\rangle), \\ |1_+ \rangle &= \frac{1}{\sqrt{2}}(|g100\rangle - \frac{\eta}{\beta_1} |g011\rangle + \frac{\eta_a}{\beta_1} |e000\rangle), \\ |2_0\rangle &= \frac{1}{A_1}(|g200\rangle + \frac{\eta_a^2 - \eta^2}{\sqrt{2}\eta^2} |g022\rangle + \frac{\sqrt{2}\eta_a}{\eta} |e011\rangle), \\ |2_{1-} \rangle &= \frac{1}{A_2}(d_{11} |g200\rangle + d_{12} |g111\rangle + d_{13} |e100\rangle \\ &\quad + d_{14} |g022\rangle + |e011\rangle), \\ |2_{1+} \rangle &= \frac{1}{A_2}(d_{11} |g200\rangle - d_{12} |g111\rangle - d_{13} |e100\rangle \\ &\quad + d_{14} |g022\rangle + |e011\rangle), \\ |2_{2-} \rangle &= \frac{1}{A_3}(d_{21} |g200\rangle + d_{22} |g111\rangle + d_{23} |e100\rangle \\ &\quad + d_{24} |g022\rangle + |e011\rangle), \\ |2_{2+} \rangle &= \frac{1}{A_3}(d_{21} |g200\rangle - d_{22} |g111\rangle - d_{23} |e100\rangle \\ &\quad + d_{24} |g022\rangle + |e011\rangle), \end{aligned} \quad (\text{A6})$$

with the coefficients: $A_1 = \frac{\sqrt{\beta_1^4 + 2\eta^4}}{\sqrt{2}\eta^2}$, $d_{11} = \frac{\beta_1^2(D - 5\eta^2 - \eta_a^2)}{\sqrt{2}\eta_a \eta M_1}$, $d_{12} = \frac{\beta_2(-5\beta_1^2 + D)}{2\eta_a M_1}$, $d_{13} = \frac{\beta_2(\beta_1^2 - D)}{2\eta M_1}$, $d_{14} = \frac{\eta(D - 5\beta_1^2)}{\eta_a M_1}$, $d_{21} = -\frac{\beta_1^2(D + 5\eta^2 + \eta_a^2)}{\sqrt{2}\eta_a \eta M_2}$, $d_{22} = -\frac{\beta_3(5\beta_1^2 + D)}{2\eta_a M_2}$, $d_{23} = \frac{\beta_2(\beta_1^2 + D)}{2\eta M_2}$, $d_{24} = -\frac{\eta(D + 5\beta_1^2)}{\eta_a M_2}$, $M_1 = 3\beta_1^2 - D$, $M_2 = 3\beta_1^2 + D$, and $A_{2(3)} = \sqrt{|d_{1(2)1}|^2 + |d_{1(2)2}|^2 + |d_{1(2)3}|^2 + |d_{1(2)4}|^2 + 1}$.

Appendix B: The dynamic equation and steady states solution

In this appendix, we derive probability amplitude for a steady state. Substitute the $|\psi\rangle$ expressed by Eq. (5) into the Schrödinger equation:

$$i \frac{\partial}{\partial t} |\psi\rangle = H_{eff} |\psi\rangle,$$

and we obtain the differential equations as

$$\begin{aligned}
i\dot{C}_{g000} &= 0, \\
i\dot{C}_{g100} &= \tilde{\Delta}C_{g100} - \eta C_{g011} + \eta_a C_{e000}, \\
i\dot{C}_{g011} &= -\eta C_{g100} + \tilde{\Delta}C_{g011}, \\
i\dot{C}_{e000} &= \eta_a C_{g100} + \tilde{\Delta}C_{e000} + \Omega_e C_{g000}, \\
i\dot{C}_{g200} &= 2\tilde{\Delta}C_{g200} - \sqrt{2}\eta C_{g111} + \sqrt{2}\eta_a C_{e100}, \\
i\dot{C}_{g111} &= -\sqrt{2}\eta C_{g200} + 2\tilde{\Delta}C_{g111} - 2\eta C_{g022} + \eta_a C_{e011}, \\
i\dot{C}_{e100} &= \Omega_e C_{g100} + \sqrt{2}\eta_a C_{g200} + 2\tilde{\Delta}C_{e100} - \eta C_{e011}, \\
i\dot{C}_{g022} &= -2\eta C_{g111} + 2\tilde{\Delta}C_{g022}, \\
i\dot{C}_{e011} &= \Omega_e C_{g011} + \eta_a C_{g111} - \eta C_{e100} + 2\tilde{\Delta}C_{e011},
\end{aligned} \tag{B1}$$

where for simplicity, we set $\kappa_+ = \kappa_- = \kappa_e = \kappa$, $\tilde{\Delta} = \Delta - i\kappa$ and temporarily ignore the small mechanical decay rate $\kappa_b \ll \kappa$, and the jumping from high level to low level is ignored as it is done in Ref. [25].

The steady-state solution of Eq. (B1) is derived as

$$\begin{aligned}
C_{g000} &= 1, \\
C_{g100} &= \frac{\eta_a \Omega_e}{\tilde{\Delta}^2 - \eta_a^2 - \eta^2}, \\
C_{g011} &= \frac{\eta \eta_a \Omega_e}{\tilde{\Delta}(\tilde{\Delta}^2 - \eta_a^2 - \eta^2)}, \\
C_{e000} &= -\frac{(\tilde{\Delta}^2 - \eta^2)\Omega_e}{\tilde{\Delta}(\tilde{\Delta}^2 - \eta_a^2 - \eta^2)}, \\
C_{g111} &= \frac{\eta_a^2 \eta (5\tilde{\Delta}^2 - \eta_a^2 + \eta^2)\Omega_e^2}{\tilde{\Delta} B}, \\
C_{g200} &= \frac{\eta_a^2 (4\tilde{\Delta}^4 + \tilde{\Delta}^2(\eta^2 - \eta_a^2) - 2\eta^4)\Omega_e^2}{\sqrt{2}\tilde{\Delta}^2 B}, \\
C_{e100} &= \frac{\eta_a (4\tilde{\Delta}^4 - \tilde{\Delta}^2(\eta_a^2 + 4\eta^2) + \eta^2\eta_a^2 - 3\eta^4)\Omega_e^2}{\tilde{\Delta} B}, \\
C_{g022} &= \frac{\eta^2 \eta_a^2 (5\tilde{\Delta}^2 - \eta_a^2 + \eta^2)\Omega_e^2}{\tilde{\Delta}^2 B}, \\
C_{e011} &= -\frac{\eta_a \eta (6\tilde{\Delta}^4 - \tilde{\Delta}^2(\eta_a^2 + 9\eta^2) + 2\eta^2\eta_a^2)\Omega_e^2}{\tilde{\Delta}^2 B},
\end{aligned} \tag{B2}$$

where $B = \frac{1}{2}(\tilde{\Delta}^2 - \beta_1^2)(4\tilde{\Delta}^2 - \beta_2^2)(4\tilde{\Delta}^2 - \beta_3^2)$.

Appendix C: The deduction of the relations between two bases

In this Appendix, we provide the certification of Eq. (8). We define the Fock basis of the supermode a_{\pm} as $|n_+ n_-\rangle_d$ and the bare modes of a and m as $|nm\rangle$. For the supermodes, we have

$$\begin{aligned}
a_+^\dagger |n_+ n_-\rangle_d &= \sqrt{n_+ + 1} |n_+ + 1 n_-\rangle_d, \\
a_+ |n_+ n_-\rangle_d &= \sqrt{n_+} |n_+ - 1 n_-\rangle_d, \\
a_-^\dagger |n_+ n_-\rangle_d &= \sqrt{n_- + 1} |n_+ n_- + 1\rangle_d, \\
a_- |n_+ n_-\rangle_d &= \sqrt{n_-} |n_+ n_- - 1\rangle_d,
\end{aligned} \tag{C1}$$

Specifically, for $n_+, n_- = 0$, we have the relation of the annihilation operator

$$a_{\pm}|00\rangle_d = 0.$$

Since $a_{\pm} = \frac{1}{\sqrt{2}}(a \pm m)$, we have $a|00\rangle_d = 0$, $m|00\rangle_d = 0$. We expand the state $|00\rangle_d$ by using the bare basis $|n, m\rangle$ of mode a and m as

$$\begin{aligned}
|00\rangle_d &= \sum_{n,m} C_{nm} |nm\rangle \\
&= C_{00}|00\rangle + C_{10}|10\rangle + C_{01}|01\rangle + \dots
\end{aligned} \tag{C2}$$

Thus

$$C_{nm} = \langle nm|00\rangle_d,$$

for example $C_{10} = \langle 10|00\rangle_d = \langle 00|a|00\rangle_d = 0$. Finally, we have

$$|00\rangle_d = |00\rangle. \tag{C3}$$

In addition, we can write $a_+^\dagger|00\rangle_d = |10\rangle_d$, i.e., $1/\sqrt{2}(a^\dagger + m^\dagger)|00\rangle = 1/\sqrt{2}(|10\rangle + |01\rangle)$. Then, we can obtain

$$|10\rangle_d = \frac{1}{\sqrt{2}}(|10\rangle + |01\rangle). \tag{C4}$$

Similarly, we can have

$$|01\rangle_d = \frac{1}{\sqrt{2}}(|10\rangle - |01\rangle). \tag{C5}$$

Taking action $a_{\pm}^\dagger = 1/\sqrt{2}(a^\dagger \pm m^\dagger)$ further on the right and left sides of Eq. (C4) and Eq. (C5), we can reach the other relations.

-
- [1] K. M. Birnbaum, A. Boca, R. Miller, A. D. Boozer, T. E. Northup, and H. J. Kimble, *Nature* **436**, 87 (2005).
[2] A. Imamoglu, H. Schmidt, G. Woods, and M. Deutsch, *Phys. Rev. Lett.* **79**, 1467 (1997).
[3] B. Hacker, S. Welte, G. Rempe, and S. Ritter, *Nature* **536**, 193 (2016).

- [4] J.-F. Huang, J.-Q. Liao, and C. P. Sun, *Phys. Rev. A* **87**, 023822 (2013).
[5] W.-W. Deng, G.-X. Li, and H. Qin, *Phys. Rev. A* **91**, 043831 (2015).
[6] C. J. Zhu, Y. P. Yang, and G. S. Agarwal, *Phys. Rev. A* **95**, 063842 (2017).

- [7] B. Dayan, A. S. Parkins, T. Aoki, E. P. Ostby, K. J. Vahala, and H. J. Kimble, *Science* **319**, 1062 (2008).
- [8] H. J. Snijders, J. A. Frey, J. Norman, H. Flayac, V. Savona, A. C. Gossard, J. E. Bowers, M. P. van Exter, D. Bouwmeester, and W. Löffler, *Phys. Rev. Lett.* **121**, 043601 (2018).
- [9] O. Arcizet, P.-F. Cohadon, T. Briant, M. Pinard, A. Heidmann, J.-M. Mackowski, C. Michel, L. Pinard, O. Francais, and L. Rousseau, *Phys. Rev. Lett.* **97**, 133601 (2006).
- [10] M. Tsang and C. M. Caves, *Phys. Rev. Lett.* **105**, 123601 (2010).
- [11] S. Nimmrichter, K. Hornberger, and K. Hammerer, *Phys. Rev. Lett.* **113**, 020405 (2014).
- [12] W.-Z. Zhang, Y. Han, B. Xiong, and L. Zhou, *New Journal of Physics* **19**, 083022 (2017).
- [13] J.-Q. Liao and L. Tian, *Phys. Rev. Lett.* **116**, 163602 (2016).
- [14] K. Stannigel, P. Komar, S. J. M. Habraken, S. D. Bennett, M. D. Lukin, P. Zoller, and P. Rabl, *Phys. Rev. Lett.* **109**, 013603 (2012).
- [15] Y.-D. Wang and A. A. Clerk, *New Journal of Physics* **14**, 105010 (2012).
- [16] Y.-C. Liu, Y.-F. Xiao, Y.-L. Chen, X.-C. Yu, and Q. Gong, *Phys. Rev. Lett.* **111**, 083601 (2013).
- [17] Z. Shen, Y.-L. Zhang, Y. Chen, C.-L. Zou, Y.-F. Xiao, X.-B. Zou, F.-W. Sun, G.-C. Guo, and C.-H. Dong, *Nature Photonics* **10**, 657 (2016).
- [18] A. Ridolfo, M. Leib, S. Savasta, and M. J. Hartmann, *Phys. Rev. Lett.* **109**, 193602 (2012).
- [19] W.-Z. Zhang, J. Cheng, J.-Y. Liu, and L. Zhou, *Phys. Rev. A* **91**, 063836 (2015).
- [20] X. Li, W.-Z. Zhang, B. Xiong, and L. Zhou, *Scientific Reports* **6**, 39343 (2016).
- [21] P. Rabl, *Phys. Rev. Lett.* **107**, 063601 (2011).
- [22] J.-Q. Liao and F. Nori, *Phys. Rev. A* **88**, 023853 (2013).
- [23] L. Zhou, J. Cheng, Y. Han, and W. Zhang, *Phys. Rev. A* **88**, 063854 (2013).
- [24] M. Ludwig, A. H. Safavi-Naeini, O. Painter, and F. Marquardt, *Phys. Rev. Lett.* **109**, 063601 (2012).
- [25] P. Kómár, S. D. Bennett, K. Stannigel, S. J. M. Habraken, P. Rabl, P. Zoller, and M. D. Lukin, *Phys. Rev. A* **87**, 013839 (2013).
- [26] C. Vaneph, A. Morvan, G. Aiello, M. Féchant, M. Aprili, J. Gabelli, and J. Estève, *Phys. Rev. Lett.* **121**, 043602 (2018).
- [27] X. Zhang, C.-L. Zou, L. Jiang, and H. X. Tang, *Phys. Rev. Lett.* **113**, 156401 (2014).
- [28] J. Bourhill, N. Kostylev, M. Goryachev, D. L. Creedon, and M. E. Tobar, *Phys. Rev. B* **93**, 144420 (2016).
- [29] M. Goryachev, W. G. Farr, D. L. Creedon, Y. Fan, M. Kostylev, and M. E. Tobar, *Phys. Rev. Applied* **2**, 054002 (2014).
- [30] X. Zhang, N. Zhu, C.-L. Zou, and H. X. Tang, *Phys. Rev. Lett.* **117**, 123605 (2016).
- [31] J. A. Haigh, A. Nunnenkamp, A. J. Ramsay, and A. J. Ferguson, *Phys. Rev. Lett.* **117**, 133602 (2016).
- [32] A. Osada, R. Hisatomi, A. Noguchi, Y. Tabuchi, R. Yamazaki, K. Usami, M. Sadgrove, R. Yalla, M. Nomura, and Y. Nakamura, *Phys. Rev. Lett.* **116**, 223601 (2016).
- [33] T. Niemczyk, F. Deppe, H. Huebl, E. Menzel, F. Hocke, M. Schwarz, J. Garcia-Ripoll, D. Zueco, T. Hümmer, E. Solano, *et al.*, *Nature Physics* **6**, 772 (2010).
- [34] J. Li, S.-Y. Zhu, and G. S. Agarwal, *Phys. Rev. Lett.* **121**, 203601 (2018).
- [35] X. Zhang, C.-L. Zou, L. Jiang, and H. X. Tang, *Sci. Adv.* **2**, e1501286 (2016).
- [36] Y.-P. Gao, C. Cao, T.-J. Wang, Y. Zhang, and C. Wang, *Phys. Rev. A* **96**, 023826 (2017).
- [37] Y.-P. Gao, X.-F. Liu, T.-J. Wang, C. Cao, and C. Wang, *Phys. Rev. A* **100**, 043831 (2019).
- [38] H. Flayac and V. Savona, *Phys. Rev. A* **96**, 053810 (2017).
- [39] H. Z. Shen, Y. H. Zhou, and X. X. Yi, *Phys. Rev. A* **90**, 023849 (2014).
- [40] A. Majumdar and D. Gerace, *Phys. Rev. B* **87**, 235319 (2013).
- [41] F. Zou, L.-B. Fan, J.-F. Huang, and J.-Q. Liao, *Phys. Rev. A* **99**, 043837 (2019).
- [42] Z.-X. Liu, H. Xiong, and Y. Wu, *Phys. Rev. B* **100**, 134421 (2019).
- [43] T. Tashima, H. Morishita, and N. Mizuochi, *Phys. Rev. A* **100**, 023801 (2019).
- [44] H. Huebl, C. W. Zollitsch, J. Lotze, F. Hocke, M. Greifenstein, A. Marx, R. Gross, and S. T. B. Goennenwein, *Phys. Rev. Lett.* **111**, 127003 (2013).
- [45] Y.-P. Wang, G.-Q. Zhang, D. Zhang, T.-F. Li, C.-M. Hu, and J. Q. You, *Phys. Rev. Lett.* **120**, 057202 (2018).
- [46] P. Hyde, B. M. Yao, Y. S. Gui, G.-Q. Zhang, J. Q. You, and C.-M. Hu, *Phys. Rev. B* **98**, 174423 (2018).
- [47] D. Zhang, X.-Q. Luo, Y.-P. Wang, T.-F. Li, and J. You, *Nature communications* **8**, 1368 (2017).
- [48] M. O. Scully and M. S. Zubairy, *Quantum optics* (Cambridge University Press, Cambridge, 1997).
- [49] M.-A. Lemonde, N. Didier, and A. A. Clerk, *Phys. Rev. A* **90**, 063824 (2014).
- [50] X. Wang, A. Miranowicz, H.-R. Li, and F. Nori, *Phys. Rev. A* **93**, 063861 (2016).
- [51] X.-W. Xu, H.-Q. Shi, J.-Q. Liao, and A.-X. Chen, *Phys. Rev. A* **100**, 053802 (2019).
- [52] X.-W. Xu, A.-X. Chen, and Y.-x. Liu, *Phys. Rev. A* **94**, 063853 (2016).
- [53] A. H. Safavi-Naeini, T. P. M. Alegre, J. Chan, M. Eichenfield, M. Winger, Q. Lin, J. T. Hill, D. E. Chang, and O. Painter, *Nature* **472**, 69 (2011).
- [54] J. B. Clark, F. Lecocq, R. W. Simmonds, J. Aumentado, and J. D. Teufel, *Nature* **541**, 191 (2017).